Accuracy of Entanglement Detection via Artificial Neural Networks and Human-Designed Entanglement Witnesses

Jan Roik,[1,*] Karol Bartkiewicz,[1,2,†] Antonín Černoch,[1,‡] and Karel Lemr[1,§]

[1] *RCPTM, Joint Laboratory of Optics of Palacký University and Institute of Physics of Czech Academy of Sciences, 17. listopadu 12, Olomouc 771 46, Czech Republic*

[2] *Institute of Spintronics and Quantum Information, Faculty of Physics, Adam Mickiewicz University, Poznań PL-61-614, Poland*

(Received 23 November 2020; revised 22 February 2021; accepted 1 April 2021; published 4 May 2021)

The detection of entangled states is essential in both fundamental and applied quantum physics. However, this task proves to be challenging, especially for general quantum states. One can execute full state tomography but this method is time demanding, especially in complex systems. Other approaches use entanglement witnesses: these methods tend to be less demanding but lack reliability. Here, we demonstrate that artificial neural networks (ANNs) provide a balance between the two approaches. In this paper, we make a comparison of ANN performance with witness-based methods for random general two-qubit quantum states without any prior information on the states. Furthermore, we apply our approach to a real experimental data set.

DOI: 10.1103/PhysRevApplied.15.054006

I. INTRODUCTION

Quantum entanglement is an intriguing phenomenon described almost a century ago by Schrödinger, Einstein, Podolsky, and Rosen [1,2]. Since then, many theoretical and practical papers alike, as well as lively discussions, have been dedicated to this topic [3–5]. The ability to effectively detect an entangled state has become essential mainly because of their application potential in quantum computing [6], quantum cryptography [7], and quantum teleportation experiments [8]. The most robust way of detecting it is via full state tomography and density-matrix estimation [9]. This method allows us to obtain all the information about the state and thus correctly detect entanglement. Unfortunately, this method is experimentally demanding because the number of required projections grows exponentially with the dimension of the Hilbert space. There is also a variety of other methods that do not rely on full state tomography [10–30]. These methods include a wide range of linear entanglement witnesses [11–16] of the Clauser-Horne-Shimony-Holt (CHSH) type [10]. While for pure states these methods give similar results, their outcomes might vary significantly when mixed states are considered. While requiring only relatively few measurement configurations, these witnesses cannot function reliably without some a prior information about the detected state. To circumvent this limitation, while not resorting to quantum state tomography (QST), nonlinear entanglement witnesses have been proposed.

In 2011, Rudnicki *et al.* introduced a nonlinear entanglement witness called *collectibility* [24,26]. For a visual demonstration of this concept, see Fig. 1(a). For two-qubit states, this witness requires two simultaneously prepared copies of the investigated state. Then, a Bell-state projection is imposed on a pair of corresponding qubits from each copy and the remaining qubits are subjected to local measurements. For a general two-qubit state, this requires a combination of five local projections and, thus, a smaller measurement configuration than full quantum state tomography, which includes at least 24 projections. One can further decrease the time needed for a QST if the measurements can be performed in parallel on multiple copies of the investigated state. When dealing with unknown quantum states, collectibility can detect a much broader range of states compared to linear witnesses. Namely, it detects all pure entangled states. Unfortunately, it detects entanglement of only a fraction of mixed states. This shortcoming is characterized by a rather large type-II error (false negative), as we show later. On the other hand, all states that are classified as entangled by this method are classified correctly (the type-I error is null; there are no false-positive classifications). We demonstrate that a significant improvement can be achieved when the collective entanglement witnesses are devised using an artificial neural network. As demonstrated by Gao *et al.* [31] and other groups

*jan.roik@upol.cz
†karol.bartkiewicz@upol.cz
‡antonin.cernoch@upol.cz
§k.lemr@upol.cz

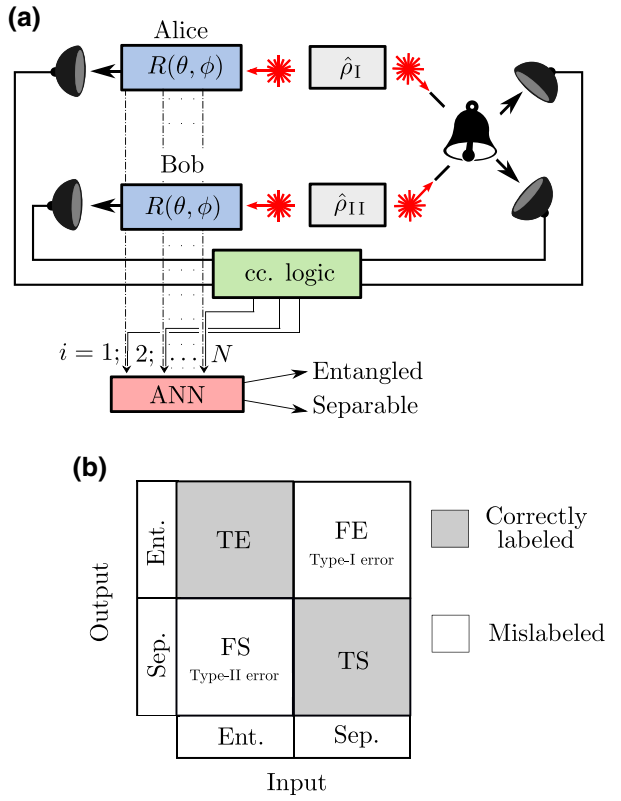

FIG. 1. (a) The scheme of the collectibility measurement: Two copies, $\hat{\rho}_{\mathrm{I}}$ and $\hat{\rho}_{\mathrm{II}}$, of the same quantum state are generated. One qubit from each pair is measured locally, while the remaining qubits are subjected to Bell measurement. The collectibility is then calculated analytically from the obtained coincidence detections. Alternatively, as we investigate in this paper, coincidence counts (cc. logic) can be fed to an artificial neural network (ANN), which then labels the states. (b) A schematic depiction of the confusion matrix used for performance evaluation of the ANN: TE, truly entangled; FE, falsely entangled; TS, truly separable; FS, falsely separable; Sep., separable; Ent., entangled.

[32,33], neural networks can be used to identify quantum states. However, only linear entanglement witnesses have been considered, which has significantly limited the class of detected entangled states. Note that neural-network-based linear witnesses share the same shortcoming with their analytical counterparts, namely the need for *a priori* information about the investigated state.

We train a neural network to classify quantum states by providing it with the results of collective measurements and demonstrate its significantly better performance over collectibility and other similar nonlinear witnesses for a general two-qubit state as well as for real experimental data for a fixed number of measurement configurations [see Fig. 1(a)]. Moreover, we show the increasing capability of the neural network when provided with a larger amount of measurement-configuration outcomes by comparing it with three other analytical methods that require 12 projections, namely the fully entangled fraction (FEF) [34–36], the CHSH [10], and the entropic witness (EW) [37,38]. These projections are listed in the Appendix. We use the confusion matrix as a method of performance evaluation for the ANN and previously known nonlinear witnesses [see Fig. 1(b)]. The diagonal elements show the number of correctly labeled truly entangled (TE) and truly separable (TS) input states: furthermore, the off-diagonal elements provide information about falsely labeled, i.e., falsely entangled (FE) and falsely separable (FS), input states.

II. NEURAL NETWORK

Random two-qubit states $\hat{\rho}_{\mathrm{I}}$ are generated (for more details, see the Appendix). The state of two copies of $\hat{\rho}_{\mathrm{I}}$ copies is described by the density matrix $\hat{\rho}_{\mathrm{I}} \otimes \hat{\rho}_{\mathrm{II}}$, where $\hat{\rho}_{\mathrm{II}}$ is derived from $\hat{\rho}_{\mathrm{I}}$ by swapping subsystems. Subsequently, the density matrix is subjected to projective measurements and probabilities are obtained:

$$P_{xy} = \frac{\mathrm{Tr}[(\hat{\rho}_{\mathrm{I}} \otimes \hat{\rho}_{\mathrm{II}})\left(\hat{\Pi}_x \otimes \hat{\Pi}_{\mathrm{Bell}} \otimes \hat{\Pi}_y\right)]}{\mathrm{Tr}[(\hat{\rho}_{\mathrm{I}} \otimes \hat{\rho}_{\mathrm{II}})\left(\hat{\Pi}_x \otimes \hat{\mathbb{1}}^{(4)} \otimes \hat{\Pi}_y\right)]}, \qquad (1)$$

where $\hat{\Pi}_x$ and $\hat{\Pi}_y$ are local projections onto single-qubit states $|x\rangle$ and $|y\rangle$, $\hat{\Pi}_{\mathrm{Bell}}$ denotes projection onto the singlet Bell state, and $\hat{\mathbb{1}}^{(4)}$ represents the four-dimensional identity matrix. The obtained set of N probabilities $P_{xy}^{(i)}$; $i = 1, \ldots, N$, is subsequently fed to a neural network for training together with labels obtained by the positive partial transpose (PPT) Peres-Horodecki criterion [39,40].

TensorFlow 2.0 [41] is used to program a neural network capable of classifying quantum states. The Supplemental Material [42] contains the source codes, the experimental data, and the parameters of the artificial neural networks. We experiment with the complexity of the network and our final layout of the network, with five hidden layers containing 36, 180, 75, 180, and 75 nodes, respectively, seems to be the optimal choice to find a balance between the obtained precision and the computation time. The proposed network is capable of assigning any quantum state with a value $w \in [0; 1]$, which can be interpreted as a confidence factor from 0 (certainly entangled) to 1 (certainly separable). We define the decision threshold ϵ to convert the w values to a binary label: $w < \epsilon \Rightarrow$ entangled and $w \geq \epsilon \Rightarrow$ separable. By changing the ϵ value, we make the network biased toward the desired decision, which allows us to tune the trade-off between type-I and type-II errors. The network is trained on 4×10^6 samples and tested on the other 4×10^5 samples with a distribution containing 67.74% entangled states and 32.26% separable states. For more details about the purity distribution of the samples, see the Appendix. The main goal is to test the network against collectibility; therefore, we start to train it using

the same $N = 5$ projection settings (for a brief overview on collectibility, see the Appendix). In the next step, we also test the capability of the network for $N = 3, 6, 12, 15$ projection settings (for more details, see the Appendix).

III. RESULTS

In the first step, we decide to test the neural network with the decision threshold $\epsilon = 0.5$ for a number of projection settings $N = 3, 5, 6, 12, 15$ (see Table II in Appendix for details). As it turns out, the neural network is capable of labeling entangled and separable states even using three projection settings, with an overall success rate of around 83.33%. For an increasing number of projection settings, the success rate increases even further and reaches 96.55% for 15 projection settings. We plot the probability of an incorrect decision as a function of the smallest eigenvalue of the partially transposed density matrix $\hat{\rho}$ (see Fig. 2).

As expected, the neural network struggles with the states close to the PPT decision boundary (minimal eigenvalue close to zero). Unfortunately, the neural network is, to some extent, prone to type-I errors (separable state classified as entangled). As it turns out, the network is more likely to make a mistake when classifying separable states than entangled states. Our solution is to change the decision threshold ϵ to decrease the type-I error. This means that we demand more certainty from the network when classifying the entangled state. By optimizing the thresholds, we manage to find the value that satisfies a condition of type-I error $< 1\%$, which we find acceptable. It is possible to arbitrarily decrease the type-I error by sacrificing the detection capability, which is characterized by type-II error. For more details on the dependence of type-I and type-II errors on the threshold for $N = 3, 5, 6, 12, 15$, see Figs. 3 and 4 and Table III. In the next step, we compare the network performance with the collectibility. The neural network fed by outcomes of the same five projection settings also required by the collectibility is able to correctly classify 78.14% of all states while committing a type-I error of 0.96% ($\epsilon = 0.9$). This performance vastly surpasses the capability of collectibility, which identifies only 36.59% of the states correctly (see Table I). To further highlight the potential of the ANN, we compare its performance with analytical methods (the FEF, the CHSH, and the EW) (see Table I). The success rate of the ANN surpasses the capabilities of the FEF by 6.01%, the EW by 34.01%, and the CHSH by 46.01% while committing a type-I error of 0.24%. This means that if we can accept some type-I error, it is possible to achieve a major improvement in the detection of entangled states using the neural network. Note that the purpose of this research is not to use the ANN simply to fit existing entanglement witnesses but, rather, to devise witnesses that we later compare with these already known analytical formulas.

We investigate the possibility of deriving approximate analytical formulas from the parameters of trained ANNs. This is a rather complex task and we are only able to find a

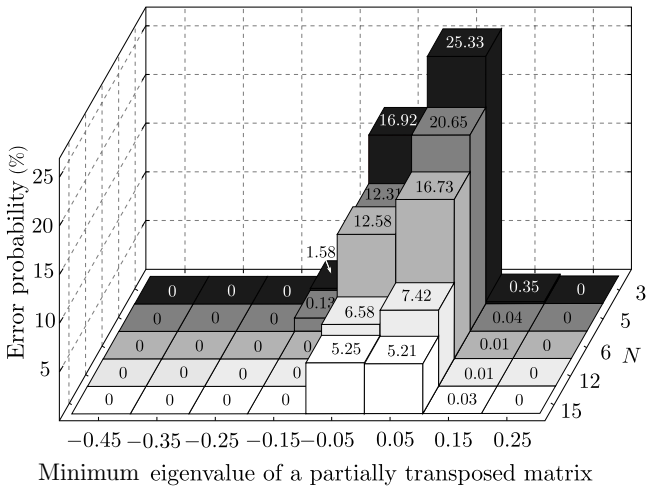

FIG. 2. The result obtained by the neural network with decision threshold $\epsilon = 0.5$ for $N = 3, 5, 6, 12, 15$ and a distribution containing 67.74% entangled states and 32.26% separable states. In this graph, the probability of false prediction is plotted against the minimal eigenvalue of a partially transposed matrix.

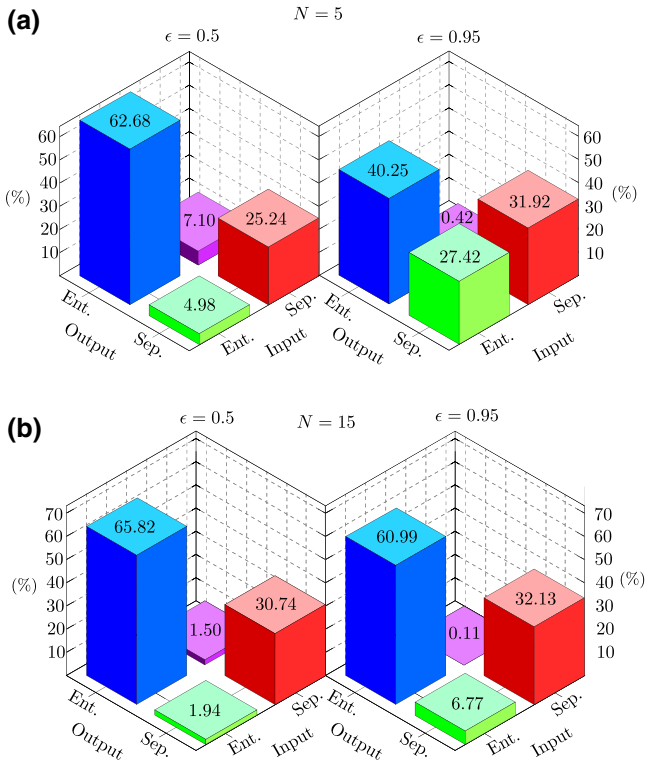

FIG. 3. The performance dependence of the ANN on the decision threshold $\epsilon = 0.5, 0.95$ with a distribution containing 67.74% entangled states and 32.26% separable states depicted as confusion matrices for (a) $N = 5$ and (b) $N = 15$.

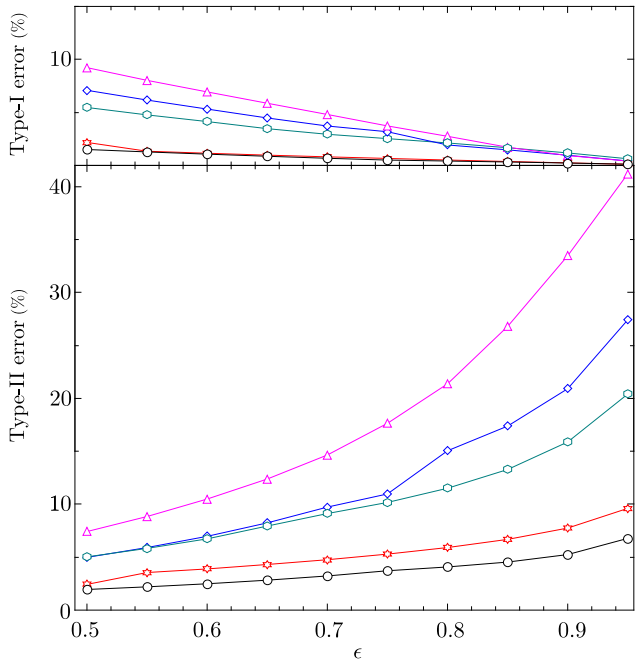

FIG. 4. The dependence of type-I and type-II errors on the ϵ threshold for varying numbers of projections: three projections, $N = 3$ ($\triangle$), five projections $N = 5$ ($\Diamond$), six projections $N = 6$ ($\bigcirc$), 12 projections $N = 12$ ($\star$), and 15 projections $N = 15$ ($\bigcirc$).

reasonable formula for the $N = 3, 5$ measurement configurations. Using logistic regression, a witness in the form of

$$W_N = \left[1 + e^{-z_N}\right]^{-1}, \tag{2}$$

where $z_N = \vec{w}_N \cdot \vec{p}_N$ and $\vec{p} = (1, P_{HH}, P_{VV}, P_{HV}, P_{DD}, P_{AA})$ for $\vec{w}_3 = (-2.3348, 19.3139, 21.5486, -11.4228, 0, 0)$ and $\vec{w}_5$=(0.0009, 7.7967, 9.6227,−25.8294, 21.9635, 22.0167), can be obtained. The states for which $W_N < 0.05$ are classified as entangled (separable otherwise). This decision boundary implies a type-I error of approximately 0.9% and type-II errors of 57.5% and 44.8%, corresponding to $N = 3, 5$, respectively. The type-I errors can be made arbitrarily small by lowering the threshold value of W_N for classifying a given state as entangled.

IV. EXPERIMENTAL IMPLEMENTATION

To verify the network capability, we decide to further test it on a set of real experimental data. For this purpose, we use the data set from the first-ever collectibility measurement from 2016 [43]. In that particular experiment, a class of Werner states of the form of $\hat{\rho}_w = p|\psi^-\rangle\langle\psi^-| + (1-p)\hat{\mathbb{1}}/4$, was investigated. $|\psi^-\rangle$ represents the singlet Bell state and $\hat{\mathbb{1}}/4$ denotes the maximally mixed state. We set the detection threshold to $\epsilon = 0.9$, as in the previous comparisons of the neural network with collectibility, to be consistent and to make the test conditions as fair as possible. The results show that collectibility can classify states with $p > 0.89$ as entangled, which corresponds with the theoretical prediction. The neural network, on the other hand, detects entangled states when $p > 0.44$ (see Fig. 5). Note that it is known that Werner states are entangled for $p > \frac{1}{3}$.

V. CONCLUSIONS

We train a neural network to classify general qubit states based on nonlinear collective witnesses. Our main goal is to compare the capability of this network against a prominent analytical representation of nonlinear witnesses: the collectibility. The network can classify the general two-qubit states significantly more efficiently than collectibility with a type-I error $< 1\%$. The ANN also surpasses the FEF, the CHSH, and the EW when taught on 12 projections (the same amount needed by the mentioned analytical witnesses). Increasing the number of projection settings improves the decision of the ANN even more. We further support this proposition by using the network on a real experimental data set. The network confirms its potential by correctly labeling a broad range of states where collectibility fails. Moreover, it achieves a type-I error =

TABLE I. A comparison of the results obtained by the ANN for $N = 3, 5, 6, 12, 15$ with prominent analytical methods (collectibility: FEF, fully entangled fraction; EW, entropic witness; CHSH nonlocality). Both type-I and type-II errors are taken for the decision threshold $\epsilon = 0.9$ to ensure a type-I error $< 1\%$.

			ANN		
N	3	5	6	12	15
Type-I error (%)	0.93	0.96	1.18	0.24	0.22
Type-II error (%)	33.47	20.91	15.88	7.74	5.24
Success rate (%)	65.50	78.14	82.94	92.01	94.54
	Collectibility	FEF	EW	CHSH	
N	5	12	12	12	
Type-I error (%)	0	0	0	0	
Type-II error (%)	63.41	14.00	42.00	54.00	
Success rate (%)	36.59	86.00	58.00	46.00	

0 on Werner states. Our research promotes the idea of using artificial intelligence toward a better understanding of intriguing physical phenomena such as entanglement. We demonstrate that the neural network can quickly train to become a valid efficient collective entanglement witness. We directly compare its performance with analytical formulas. Using nonlinear measurements (on two copies of the state), our network operates completely free of any *a priori* information that can bias the comparison of its performance with its analytical counterparts. Moreover, we show that the training performed on numerically generated states works very well on real experimental data corresponding to states completely unknown to the ANN.

Because of technical limitations on the possible complexity of our ANN and on the number of samples processed in ANN training, reaching the limit of zero type-I error is not possible. However, we are able to tune this error to a fraction of a percent by choosing a proper value of ϵ. By extrapolating our results for the whole available range of ϵ, we conclude that the limit of a vanishing type-I error is reached by the ANN for $\epsilon = 0.9822$ and $\epsilon = 0.9994$ for 5 and 12 measurements, respectively. The type-II errors for these values of ϵ are 31.26% (five measurements, about 32% better then collectibility) and 11.40% (12 measurements, 2.6% better than the FEF). Thus, we demonstrate that the best-known analytical methods for certifying entanglement with a few measurements can be further improved. Notably, the 2.6%-smaller type-I error of the ANN with respect to the FEF means that the ANN fails relatively on about 20% fewer states than the FEF using the same input. This demonstrates that there is still room for improvement in the theory of experimentally friendly entanglement detection. The extrapolation of the functional dependence of type-I and type-II errors on ϵ is performed by fitting a quadratic and an exponential curve, respectively. We believe that the high quality of both fits and the proximity of the lowest type-I error data point to 0 justify our conclusions. We hope that our results will stimulate further research in experimentally friendly methods of classifying quantum states.

Further to that, the theoretical assumption of zero type-I error of analytical witnesses does not hold operationally because of unavoidable experimental imperfections and the finite precision of all measurements. As a result, separable states close to the decision boundary may be misclassified even using theoretically infallible witnesses. In this study, we allow the ANN a type-I error of about 1%, which we believe is still an admissible error that can be tolerated in practical implementations burdened by the above-mentioned experimental imperfections. Note that in the case of 12 measurement configurations, the ANN misclassifies only 1 in about 400 separable states, while simultaneously missclassifying about half as many entangled states than its best performing analytical counterpart, the FEF.

ACKNOWLEDGMENTS

We thank Czech Education and Scientific Network for providing data management services. We acknowledge financial support by the Czech Science Foundation under Project No. 19-19002S. K.B. also acknowledges the financial support of the Polish National Science Center under Grant No. DEC-2019/34/A/ST2/00081. J.R. also acknowledges internal Palacky University Grant No. IGA_PrF_2021_004. We also acknowledge Project No. CZ.02.1.01./0.0/0.0/16_019/0000754 of the Ministry of Education, Youth and Sports of the Czech Republic.

APPENDIX: THEORETICAL FRAMEWORK

1. State sampling and numerical processing

This paper focuses on general two-qubit states. In order to correctly prepare test and training data sets, we generate diagonal elements of the 4×4 matrix M according to [44]:

$$M = \begin{pmatrix} M_{11} & 0 & 0 & 0 \\ 0 & M_{22} & 0 & 0 \\ 0 & 0 & M_{33} & 0 \\ 0 & 0 & 0 & M_{44} \end{pmatrix}, \tag{A1}$$

where $M_{11} = r_1, M_{22} = r_2(1 - M_{11}), M_{33} = r_3(1 - M_{11} - M_{22})$, $M_{44} = r_4(1 - M_{11} - M_{22} - M_{33})$, and r_n, for $n = 1, 2, 3, 4$ gives uniformly distributed random numbers in the range $[0, 1]$. The matrix is then normalized. In the next step, proper random unitary transformation is used in order to create a density matrix of a general random two-qubit state [45]:

$$U = \begin{pmatrix} 1 & 0 & 0 & 0 \\ 0 & 1 & 0 & 0 \\ 0 & 0 & \multicolumn{2}{c}{\multirow{2}{*}{U_1}} \\ 0 & 0 & & \end{pmatrix} \begin{pmatrix} 1 & 0 & 0 & 0 \\ 0 & \multicolumn{2}{c}{\multirow{2}{*}{U_2}} & 0 \\ 0 & & & 0 \\ 0 & 0 & 0 & 1 \end{pmatrix} \begin{pmatrix} \multicolumn{2}{c}{\multirow{2}{*}{U_3}} & 0 & 0 \\ & & 0 & 0 \\ 0 & 0 & 1 & 0 \\ 0 & 0 & 0 & 1 \end{pmatrix}$$
$$\begin{pmatrix} 1 & 0 & 0 & 0 \\ 0 & 1 & 0 & 0 \\ 0 & 0 & \multicolumn{2}{c}{\multirow{2}{*}{U_4}} \\ 0 & 0 & & \end{pmatrix} \begin{pmatrix} 1 & 0 & 0 & 0 \\ 0 & \multicolumn{2}{c}{\multirow{2}{*}{U_5}} & 0 \\ 0 & & & 0 \\ 0 & 0 & 0 & 1 \end{pmatrix} \begin{pmatrix} 1 & 0 & 0 & 0 \\ 0 & 1 & 0 & 0 \\ 0 & 0 & \multicolumn{2}{c}{\multirow{2}{*}{U_6}} \\ 0 & 0 & & \end{pmatrix}, \tag{A2}$$

TABLE II. The list of specific projection settings used for the training of the artificial neural network.

N	$\|i\rangle\|j\rangle$
3	$\|H\rangle\|H\rangle, \|V\rangle\|V\rangle, \|H\rangle\|V\rangle$
5	$\|H\rangle\|H\rangle, \|V\rangle\|V\rangle, \|H\rangle\|V\rangle, \|D\rangle\|D\rangle, \|A\rangle\|A\rangle$
6	$\|H\rangle\|H\rangle, \|V\rangle\|V\rangle, \|H\rangle\|V\rangle, \|D\rangle\|D\rangle, \|R\rangle\|R\rangle, \|L\rangle\|L\rangle$
12	$\|D\rangle\|D\rangle, \|A\rangle\|A\rangle, \|D\rangle\|L\rangle, \|A\rangle\|R\rangle, \|D\rangle\|H\rangle, \|A\rangle\|V\rangle,$ $\|L\rangle\|L\rangle, \|R\rangle\|R\rangle, \|L\rangle\|H\rangle, \|R\rangle\|V\rangle, \|H\rangle\|H\rangle, \|V\rangle\|V\rangle,$
15	$\|D\rangle\|D\rangle, \|A\rangle\|A\rangle, \|D\rangle\|L\rangle, \|A\rangle\|R\rangle, \|D\rangle\|H\rangle, \|A\rangle\|V\rangle, \|L\rangle\|L\rangle,$ $\|R\rangle\|R\rangle, \|L\rangle\|H\rangle, \|R\rangle\|V\rangle, \|H\rangle\|H\rangle, \|V\rangle\|V\rangle, \|D\rangle\|R\rangle, \|D\rangle\|V\rangle, \|L\rangle\|V\rangle$

TABLE III. The evolution of type-I and type-II errors for different thresholds ϵ. T-I and T-II represent type-I and type-II errors, respectively, and are listed as percentages.

N	3		5		6		12		15	
ϵ	T-I	T-II	T-I	T-II	T-I	T-II	T-I	T-II	T-I	T-II
0.5	9.23	7.42	7.09	4.98	5.47	5.03	2.17	2.43	1.50	1.94
0.55	8.03	8.84	6.17	5.91	4.77	5.83	1.34	3.55	1.27	2.19
0.6	6.94	10.49	5.32	6.97	4.14	6.73	1.15	3.89	1.06	2.48
0.65	5.87	12.38	4.48	8.24	3.47	7.94	0.97	4.31	0.86	2.82
0.7	4.81	14.65	3.72	9.73	2.94	9.12	0.81	4.76	0.67	3.22
0.75	3.73	17.64	3.18	10.97	2.53	10.17	0.66	5.29	0.50	3.71
0.8	2.75	21.37	1.93	15.05	2.12	11.51	0.51	5.91	0.41	4.07
0.85	1.72	26.79	1.47	17.38	1.67	13.28	0.37	6.68	0.32	4.53
0.9	0.93	33.47	0.96	20.91	1.18	15.88	0.24	7.75	0.22	5.24
0.95	0.41	41.21	0.42	27.42	0.63	20.41	0.11	9.61	0.11	6.77

where

$$U_j = e^{i\alpha_j} \begin{pmatrix} e^{i\psi_j}\cos\phi_j & e^{i\chi_j}\sin\phi_j \\ -e^{-i\chi_j}\sin\phi_j & e^{-i\psi_j}\cos\phi_j \end{pmatrix}, \quad j = 1,\ldots,6, \tag{A3}$$

with $0 \le \phi \le \pi/2$ and $0 \le \alpha, \psi, \chi < 2\pi$. The homogenous distribution of states is ensured by $\phi_j = \arcsin\sqrt{\xi_j}, \xi_j \in [0,1]$. The parameters ϕ_j, ψ_j, χ_j, α_j, and ξ_j are picked from their respective intervals with uniform probability [see Fig. 6 for the resulting purity statistics]. The final density matrix is obtained as $M_o = UMU^\dagger$. The training and test data are labeled via the PPT criterion [39,40]. To mathematically describe the collective measurement, a four-qubit density matrix M_f is defined as $M_f = M_o \otimes M_t$. To implement the Bell-state projection on the neighboring $(2,3)$ qubits, M_t is obtained from M_o by swapping subsystems:

$$M_t = S\, M_0\, S, \tag{A4}$$

where

$$S = \begin{pmatrix} 1 & 0 & 0 & 0 \\ 0 & 0 & 1 & 0 \\ 0 & 1 & 0 & 0 \\ 0 & 0 & 0 & 1 \end{pmatrix}. \tag{A5}$$

2. Collectibility

In order to calculate the collectibility, we used the formula of Rudnicky *et al.* [26], represented in computational bases, i.e., $H \to |0\rangle$, $V \to |1\rangle$, $D \to |+\rangle = (|0\rangle + |1\rangle)/\sqrt{2}$, $A \to |-\rangle = (|0\rangle - |1\rangle)/\sqrt{2}$, $R \to (|0\rangle - i|1\rangle)/\sqrt{2}$, and $L \to = (|0\rangle + i|1\rangle)/\sqrt{2}$:

$$W(\hat{\rho}) = \frac{1}{2}[\eta + p_0^2(1 - r_{00}) + (1-p_0)^2(1-r_{11}) + 2p_0(1-p_0)(1-r_{01}) - 1], \tag{A6}$$

where

$$\eta = 8p_0(1-p_0)\sqrt{r_{00}r_{11}} + 2p'. \tag{A7}$$

In the above equations, the single-photon projection probability $p_0 = M_{o_{00}} + M_{o_{11}}$ and $p' = \max\{p_{++}, p_{--}\}$. P_{xy} represents the probabilities of single Bell-state projection of a nonlocally measured qubit conditioned on local projection onto the $|x\rangle$ and $|y\rangle$ states [26].

3. Other two-copy witnesses

A class of two-copy entanglement witnesses can be calculated using elements of the symmetric matrix [35]

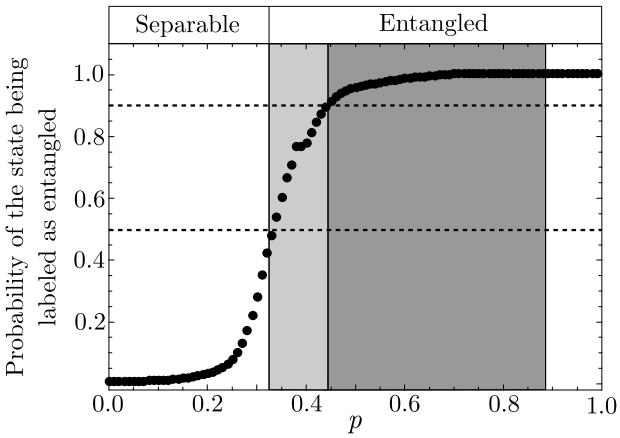

FIG. 5. The results obtained by the ANN and by collectibility, respectively, using a real experimental data set $N = 5$. The black full dots show the probability of a Werner state being labeled as entangled by the ANN. The light-gray area covers the values of p that neither the ANN nor collectibility can classify correctly. The dark-gray area represents the range of p values for which the ANN classifies the Werner states correctly and collectibility fails. The dashed lines represent the decision thresholds $\epsilon = 0.9$ and 0.5, respectively.

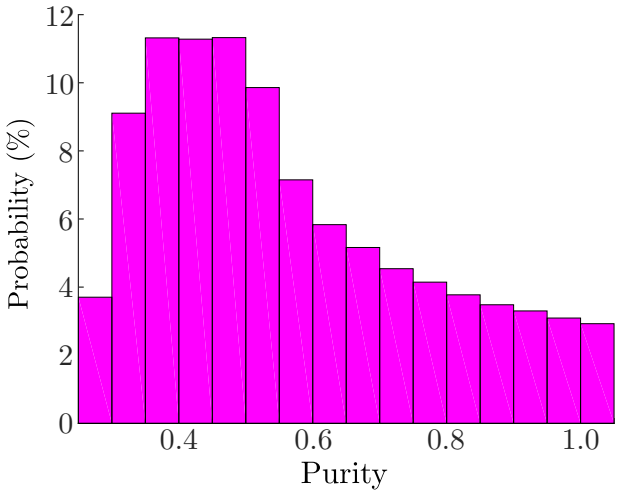

FIG. 6. The purity distribution of the training and test states.

$$R_{i,j} = R_{j,i} = \left\langle \sigma_i^{(a_1)} \otimes \sigma_j^{(a_2)} \otimes |\Psi^-_{b_1,b_2}\rangle\langle\Psi^-_{b_1,b_2}| \right\rangle, \quad \text{(A8)}$$

where the expectation values are calculated on two copies of ρ, i.e., $\rho_{a_1,b_1} \otimes \rho_{a_2,b_2}$. To estimate the number of projections, let us use the resolution of the two-qubit identity operator that is valid for an arbitrary $i,j = 1,2,3$, which reads

$$\mathbb{1}^{\otimes 2} = \sum_{r,s=0,1} |r_i s_j\rangle\langle r_i s_j|, \quad \text{(A9)}$$

where $|0_i\rangle$ and $|1_i\rangle$ are eigenstates of the σ_i operator associated with the ± 1 eigenvalues, respectively. A product of two Pauli operators reads

$$\sigma_i^{(a_1)} \otimes \sigma_j^{(a_2)} = |0_i 0_j\rangle\langle 0_i 0_j| + |1_i 1_j\rangle\langle 1_i 1_j| - (|0_i 1_j\rangle\langle 0_i 1_j| + |1_i 0_j\rangle\langle 1_i 0_j|). \quad \text{(A10)}$$

By adding the corresponding sides of Eqs. (A9) and (A10) and subtracting $\mathbb{1}^{\otimes 2}$, we obtain

$$\sigma_i^{(a_1)} \otimes \sigma_j^{(a_2)} = 2(|0_i 0_j\rangle\langle 0_i 0_j| + |1_i 1_j\rangle\langle 1_i 1_j|) - \mathbb{1}^{\otimes 2}. \quad \text{(A11)}$$

This means that the measurement all 6 different elements of R (i.e., $i \leq j$ for $i,j = 1,2,3$) requires 12 projections in total. These projections read as follows:

$$\begin{aligned} &|D\rangle|D\rangle, |A\rangle|A\rangle, |D\rangle|L\rangle, |A\rangle|R\rangle, \\ &|D\rangle|H\rangle, |A\rangle|V\rangle, |L\rangle|L\rangle, |R\rangle|R\rangle, \\ &|L\rangle|H\rangle, |R\rangle|V\rangle, |H\rangle|H\rangle, |V\rangle|V\rangle. \end{aligned} \quad \text{(A12)}$$

By using these 12 projections, we determine the matrix Q used to calculate entanglement witnesses. The fully entangled fraction f can be used to construct an entanglement witness [35]:

$$F = 2f - 1 = \tfrac{1}{2}[\mathrm{Tr}(\sqrt{Q}) - 1]. \quad \text{(A13)}$$

This and the following witnesses are positive if entanglement is detected and negative otherwise. The maximum value is 1.

Furthermore, by using an optimal CHSH inequality, we can construct an entanglement witness [35] as

$$M = \mathrm{Tr}(Q) - \min[\mathrm{eig}(Q)]. \quad \text{(A14)}$$

It is also possible to use Q to express an entropic entanglement witness: [35]

$$E = \tfrac{1}{2}[\mathrm{Tr}(Q) - 1]. \quad \text{(A15)}$$

[1] E. Schrödinger, Discussion of probability relations between separated systems, Math. Proc. Cambridge Philos. Soc. **31**, 555 (1935).

[2] A. Einstein, B. Podolsky, and N. Rosen, Can quantum-mechanical description of physical reality be considered complete? Phys. Rev. **47**, 777 (1935).

[3] M. B. Plenio and S. Virmani, in *Quantum Information and Coherence* (Springer, Heidelberg, 2014) p. 173.

[4] R. Horodecki, P. Horodecki, M. Horodecki, and K. Horodecki, Quantum entanglement, Rev. Mod. Phys. **81**, 865 (2009).

[5] F. Mintert, A. Carvalho, M. Kuś, and A. Buchleitner, Measures and dynamics of entangled states, Phys. Rep. **415**, 207 (2005).

[6] A. Steane, Quantum computing, Rep. Prog. Phys. **61**, 117 (1998).

[7] N. Gisin, G. Ribordy, W. Tittel, and H. Zbinden, Quantum cryptography, Rev. Mod. Phys. **74**, 145 (2002).

[8] D. Bouwmeester, J.-W. Pan, K. Mattle, M. Eibl, H. Weinfurter, and A. Zeilinger, Experimental quantum teleportation, Nature **390**, 575 (1997).

[9] A. Salles, F. de Melo, M. P. Almeida, M. Hor-Meyll, S. P. Walborn, P. H. Souto Ribeiro, and L. Davidovich, Experimental investigation of the dynamics of entanglement: Sudden death, complementarity, and continuous monitoring of the environment, Phys. Rev. A **78**, 022322 (2008).

[10] J. F. Clauser, M. A. Horne, A. Shimony, and R. A. Holt, Proposed Experiment to Test Local Hidden-Variable Theories, Phys. Rev. Lett. **23**, 880 (1969).

[11] K. Bartkiewicz, B. Horst, K. Lemr, and A. Miranowicz, Entanglement estimation from Bell inequality violation, Phys. Rev. A **88**, 052105 (2013).

[12] P. Horodecki, From limits of quantum operations to multicopy entanglement witnesses and state-spectrum estimation, Phys. Rev. A **68**, 052101 (2003).

[13] F. A. Bovino, G. Castagnoli, A. Ekert, P. Horodecki, C. M. Alves, and A. V. Sergienko, Direct Measurement of Nonlinear Properties of Bipartite Quantum States, Phys. Rev. Lett. **95**, 240407 (2005).

[14] A. R. R. Carvalho, F. Mintert, and A. Buchleitner, Decoherence and Multipartite Entanglement, Phys. Rev. Lett. **93**, 230501 (2004).

[15] Z.-H. Chen, Z.-H. Ma, O. Gühne, and S. Severini, Estimating Entanglement Monotones with a Generalization of the Wootters Formula, Phys. Rev. Lett. **109**, 200503 (2012).

[16] L. Aolita and F. Mintert, Measuring Multipartite Concurrence with a Single Factorizable Observable, Phys. Rev. Lett. **97**, 050501 (2006).

[17] S. P. Walborn, P. H. Souto Ribeiro, L. Davidovich, F. Mintert, and A. Buchleitner, Experimental determination of entanglement with a single measurement, Nature **440**, 1022 (2006).

[18] P. Badziag, Č. Brukner, W. Laskowski, T. Paterek, and M. Żukowski, Experimentally Friendly Geometrical Criteria for Entanglement, Phys. Rev. Lett. **100**, 140403 (2008).

[19] M. Huber, F. Mintert, A. Gabriel, and B. C. Hiesmayr, Detection of High-Dimensional Genuine Multipartite Entanglement of Mixed States, Phys. Rev. Lett. **104**, 210501 (2010).

[20] O. Gühne, M. Reimpell, and R. F. Werner, Estimating Entanglement Measures in Experiments, Phys. Rev. Lett. **98**, 110502 (2007).

[21] J. Eisert, F. G. S. L. Brandão, and K. M. R. Audenaert, Quantitative entanglement witnesses, New J. Phys. **9**, 46 (2007).

[22] R. Augusiak, M. Demianowicz, and P. Horodecki, Universal observable detecting all two-qubit entanglement and determinant-based separability tests, Phys. Rev. A **77**, 030301 (2008).

[23] A. Osterloh and P. Hyllus, Estimating multipartite entanglement measures, Phys. Rev. A **81**, 022307 (2010).

[24] L. Rudnicki, P. Horodecki, and K. Życzkowski, Collective Uncertainty Entanglement Test, Phys. Rev. Lett. **107**, 150502 (2011).

[25] B. Jungnitsch, T. Moroder, and O. Gühne, Taming Multiparticle Entanglement, Phys. Rev. Lett. **106**, 190502 (2011).

[26] L. Rudnicki, Z. Puchała, P. Horodecki, and K. Życzkowski, Collectibility for mixed quantum states, Phys. Rev. A **86**, 062329 (2012).

[27] Ł. Rudnicki, Z. Puchala, P. Horodecki, K. Życzkowski, Constructive entanglement test from triangle inequality, J. Phys. A: Math. Theor. **47**, 424035 (2014).

[28] L. Zhou and Y.-B. Sheng, Detection of nonlocal atomic entanglement assisted by single photons, Phys. Rev. A **90**, 024301 (2014).

[29] H. S. Park, S.-S. B. Lee, H. Kim, S.-K. Choi, and H.-S. Sim, Construction of an Optimal Witness for Unknown Two-Qubit Entanglement, Phys. Rev. Lett. **105**, 230404 (2010).

[30] W. Laskowski, D. Richart, C. Schwemmer, T. Paterek, and H. Weinfurter, Experimental Schmidt Decomposition and State Independent Entanglement Detection, Phys. Rev. Lett. **108**, 240501 (2012).

[31] J. Gao, L.-F. Qiao, Z.-Q. Jiao, Y.-C. Ma, C.-Q. Hu, R.-J. Ren, A.-L. Yang, H. Tang, M.-H. Yung, and X.-M. Jin, Experimental Machine Learning of Quantum States, Phys. Rev. Lett. **120**, 240501 (2018).

[32] Y.-C. Ma and M.-H. Yung, Transforming Bell's inequalities into state classifiers with machine learning, npj Quantum Inf. **4**, 34 (2018).

[33] S. Lu, S. Huang, K. Li, J. Li, J. Chen, D. Lu, Z. Ji, Y. Shen, D. Zhou, and B. Zeng, Separability-entanglement classifier via machine learning, Phys. Rev. A **98**, 012315 (2018).

[34] C. H. Bennett, D. P. DiVincenzo, J. A. Smolin, and W. K. Wootters, Mixd-state entanglement and quantum error correction, Phys. Rev. A **54**, 3824 (1996).

[35] K. Bartkiewicz, K. Lemr, A. Černoch, and A. Miranowicz, Bell nonlocality and fully entangled fraction measured in an entanglement-swapping device without quantum state tomography, Phys. Rev. A **95**, 030102 (2017).

[36] K. Bartkiewicz, P. Horodecki, K. Lemr, A. Miranowicz, and K. Życzkowski, Method for universal detection of two-photon polarization entanglement, Phys. Rev. A **91**, 032315 (2015).

[37] A. S. M. de Castro and V. V. Dodonov, Covariance measures of intermode correlations and inseparability for continuous variable quantum systems, J. Opt. B: Quantum Semiclassical Opt. **5**, S593 (2003).

[38] V. Vedral and M. B. Plenio, Entanglement measures and purification procedures, Phys. Rev. A **57**, 1619 (1998).

[39] M. Horodecki, P. Horodecki, and R. Horodecki, Separability of mixed states: Necessary and sufficient conditions, Phys. Lett. A **223**, 1 (1996).

[40] A. Peres, Separability Criterion for Density Matrices, Phys. Rev. Lett. **77**, 1413 (1996).

[41] M. Abadi, P. Barham, J. Chen, Z. Chen, A. Davis, J. Dean, M. Devin, S. Ghemawat, G. Irving, M. Isard, *et al.*, in *12th {USENIX} Symposium on Operating Systems Design and Implementation ({OSDI} 16)* (Savannah, GA, USA, 2016), p. 265, https://www.usenix.org/system/files/conference/osdi16/osdi16-abadi.pdf.

[42] The Supplemental Material at http://link.aps.org/supplemental/10.1103/PhysRevApplied.15.054006 contains the used source codes, the experimental data, and the parameters of the ANNs.

[43] K. Lemr, K. Bartkiewicz, and A. Černoch, Experimental measurement of collective nonlinear entanglement witness for two qubits, Phys. Rev. A **94**, 052334 (2016).

[44] J. Maziero, Random sampling of quantum states: A survey of methods, Braz. J. Phys. **45**, 575 (2015).

[45] C.-K. Li, R. Roberts, and X. Yin, Decomposition of unitary matrices and quantum gates, Int. J. Quantum Inf. **11**, 1350015 (2013).